Challenges and Issues of Modern Science
2026, Vol. 5, No. 1, ID 334
ISSN: 3083-5704
URL: https://cims.fti.dp.ua/j/article/view/334
DOI: https://doi.org/10.15421/cims.5.334

UDC 556.388:614.777

Integrated Hydrogeochemical and Probabilistic Health Risk Assessment of Groundwater Contamination from Brewery Effluent in Aba, Southeastern Nigeria

Chidimma Onyinye Ikeme, Stephen Obioma Akidi, Chukwuebuka Nnamdi Onwubuariri, Chidiebere Charles Agoha

Purpose. This study evaluates groundwater contamination and associated human health risks arising from brewery effluent discharge in Aba, southeastern Nigeria, with emphasis on hydrogeochemical processes and probabilistic risk characterization. **Design / Method / Approach.** Fifteen groundwater samples from wells and boreholes were analysed for arsenic (As), cadmium (Cd), cobalt (Co), chromium (Cr), nickel (Ni), and lead (Pb) using atomic absorption spectrometry under strict quality control. Hydrogeochemical facies were determined, while multivariate statistical techniques (Pearson correlation, principal component analysis, and hierarchical cluster analysis) were applied to identify contamination sources. Spatial distribution was assessed using inverse distance weighting. Health risks were evaluated using deterministic models and Monte Carlo simulation (10,000 iterations), including sensitivity analysis. **Findings.** Results revealed a hydrogeochemical shift from Ca–HCO_3 to Na–Cl facies near the effluent zone, indicating anthropogenic influence. Arsenic concentrations exceeded permissible limits in several locations. Deterministic risk assessment showed hazard index (HI) values above unity, particularly in children. Probabilistic analysis indicated elevated non-carcinogenic and carcinogenic risks, with a 95th percentile HI of 6.20 and cancer risk up to 9.8×10^{-4}. Sensitivity analysis identified arsenic as the dominant risk contributor. **Theoretical Implications.** The study advances understanding of contaminant transport mechanisms and risk variability in groundwater systems impacted by industrial effluents in developing urban environments. **Practical Implications.** Findings highlight the urgent need for effective effluent treatment, groundwater monitoring, and public health interventions in industrialized regions. **Originality / Value.** This research integrates hydrogeochemical analysis with probabilistic health risk modelling, providing a comprehensive framework for assessing industrial groundwater contamination in sub-Saharan Africa. **Research Limitations / Future Research.** The study is limited by sample size and spatial coverage. Future research should incorporate seasonal variations, larger datasets, and advanced predictive modelling approaches. **Article Type.** Empirical Paper.

Keywords:

groundwater contamination, brewery effluent, heavy metals, probabilistic health-risk assessment, multivariate statistical analysis

---

Мета. Дослідження оцінює забруднення підземних вод та ризики для здоров'я людини внаслідок скидання стічних вод пивоварні в Аба, південно-східна Нігерія, з акцентом на гідрогеохімічні процеси та імовірнісну оцінку ризику. **Дизайн / Метод / Підхід.** П'ятнадцять зразків підземних вод із криниць і свердловин проаналізовано на вміст миш'яку (As), кадмію (Cd), кобальту (Co), хрому (Cr), нікелю (Ni) та свинцю (Pb) методом атомно-абсорбційної спектрометрії із суворим контролем якості. Гідрогеохімічні фації визначено, а для ідентифікації джерел забруднення застосовано кореляційний аналіз Пірсона, аналіз основних компонент та ієрархічний кластерний аналіз. Просторовий розподіл оцінено методом зваженої відстані, ризики для здоров'я — детерміністичними моделями та методом Монте-Карло (10 000 ітерацій) з аналізом чутливості. **Результати.** Виявлено гідрогеохімічний перехід від фації Ca–HCO_3 до Na–Cl поблизу зони скидання стоків, що свідчить про антропогенний вплив. Концентрації миш'яку перевищили допустимі норми в кількох точках відбору проб. Детерміністична оцінка показала значення індексу небезпеки (HI) вище одиниці, особливо для дітей; імовірнісний аналіз підтвердив підвищені неканцерогенні та канцерогенні ризики зі значенням HI на 95-му перцентилі 6,20 та онкологічним ризиком до $9{,}8 \times 10^{-4}$. Миш'як визначено основним чинником ризику. **Теоретичне значення.** Дослідження поглиблює розуміння механізмів переносу забруднювачів та варіабельності ризику в системах підземних вод, що зазнають впливу промислових стоків в урбанізованих середовищах країн, що розвиваються. **Практичне значення.** Результати обґрунтовують нагальну потребу в ефективному очищенні стічних вод, моніторингу підземних вод та заходах охорони громадського здоров'я в промислових регіонах. **Оригінальність / Цінність.** Інтеграція гідрогеохімічного аналізу з імовірнісним моделюванням ризику для здоров'я забезпечує комплексну основу для оцінки забруднення підземних вод промисловими стоками в країнах Африки на південь від Сахари. **Обмеження дослідження / Майбутні дослідження.** Дослідження обмежене розміром вибірки та просторовим охопленням; подальші роботи мають включати сезонні варіації, більші масиви даних та вдосконалені підходи до прогностичного моделювання. **Тип статті.** Емпірична.

Ключові слова:

забруднення підземних вод, стічні води пивоварні, важкі метали, імовірнісна оцінка ризику для здоров'я, багатовимірний статистичний аналіз

Contributor Details:

Chidimma Onyinye Ikeme, Federal University of Technology Owerri: Owerri, IMO State, NG, chidimma.ikeme@futo.edu.ng
Stephen Obioma Akidi, Michael Okpara University of Agriculture: Umudike, Abia, NG, buksgeophysical@gmail.com
Chukwuebuka Nnamdi Onwubuariri, Michael Okpara University of Agriculture: Umudike, Abia, NG, Onwubuariri.chukwuebuka@mouau.edu.ng
Chidiebere Charles Agoha, Federal University of Technology Owerri: Owerri, IMO State, NG, chidiebere.agoha@futo.edu.ng

Received: 2026-04-09 *Revised: 2026-04-16* *Accepted: 2026-04-18* *Published: 2026-04-28*

Millions of people globally rely on groundwater for drinking water, particularly in developing nations with poor municipal water systems (Gleick, 2014; Twinomucunguzi et al. 2020). However, urbanisation, industrialisation, and poor waste management are eroding these resources (Foster & Chilton, 2003). Due to their complex composition and ability to migrate through subsurface layers, industrial effluents have been proven to be a major source of groundwater pollution (Alloway, 2013).

Breweries generate large volumes of wastewater containing organic chemicals, nutrients, and trace metals from source materials, process additives, equipment corrosion, and other auxiliary inputs (Ochommadu, et al. 2025). Poor treatment or disposal can allow effluents to infiltrate into the soil and aquifers, deteriorating groundwater quality (Zhang et al., 2020). Arsenic, cadmium, chromium, nickel, cobalt, and lead are harmful to health; they persist in the environment, resist biodegradation, and accumulate in organisms (Smedley & Kinniburgh, 2017; Orosun et al., 2020).

Water contaminated with certain metals can cause renal impairment, neurological issues, cardiovascular issues, and cancer (WHO, 2017; IARC, 2012). Arsenic and hexavalent chromium are Group 1 carcinogens that cause long-term damage even at low exposures (IARC, 2012; Sims et al., 2002). Thus, heavy metal concentrations in industrially discharged groundwater and their health effects must be assessed for informed environmental control and public health protection (Li et al., 2022; Orosun, 2021).

Groundwater is the primary source of domestic water for most Nigerians (Bamigboye et al., 2025). Despite this significant use, studies on the effects of brewery effluent on groundwater are limited. Most studies have focused on surface water contamination or descriptive comparisons with acceptable levels (Ubong, et al., 2023; Orosun, 2020). Many scholars use deterministic health risk models that do not account for exposure factor uncertainty and variability, which may lead to underestimation of long-term effects (USEPA, 2011; Li et al., 2022).

Recent advances in environmental science highlight the necessity for integrated methodologies that combine hydrogeochemical characterisation, multivariate statistics, spatial analysis, and probabilistic risk modelling to explain contamination processes and health impacts (Rinklebe et al., 2019). Principal component analysis differentiates natural and human-derived metal sources (Alloway, 2013; Mukherjee et al., 2019), while spatial mapping locates pollution hotspots and sensitive locations (Zhang et al., 2020). Probabilistic models, including Monte Carlo simulations, explicitly incorporate toxicity and exposure variable uncertainty to improve risk estimation (Orosun, 2021; Li et al., 2022).

This study investigates groundwater contamination and associated health risks in Aba, southeastern Nigeria, arising from brewery wastewater. **The objectives are** to determine the concentrations of heavy metals in groundwater and their spatial patterns; identify key geochemical controls and pollution sources using statistical methods; assess non-carcinogenic and carcinogenic risks using deterministic and probabilistic methods; and produce spatially defined risk maps to support groundwater management and policy decisions. **The aim of this study** is to evaluate the impact of brewery effluent on groundwater quality and associated human health risks using an integrated hydrogeochemical and probabilistic risk assessment framework. This research uses an integrated and uncertainty-aware approach to fill research gaps and offer scientifically robust insights into industrially affected groundwater systems in sub-Saharan Africa.

Study Area and Hydrogeological Setting

The research was carried out in Aba, a significant industrial and commercial city in southeastern Nigeria, in the transitional area between the Niger Delta Basin and the Anambra Basin. Aba is situated at latitudes 5.11° N to 5.13° N and longitudes 7.36° E to 7.38° E, having undergone significant urban and industrial growth in the past thirty years. The city hosts various manufacturing industries, including breweries, which produce significant amounts of liquid effluents. The regional climate is classified as humid tropical, characterised by a bimodal rainfall pattern, with mean annual precipitation surpassing 2,000 mm and average temperatures between 26 and 30°C. Intense rainfall enhances groundwater recharge while concurrently elevating the vulnerability of shallow aquifers to contamination via leaching and infiltration mechanisms (Benkhelil, 1989; Kabir et al., 2021; Onwubuariri, et al., 2025).

The study area is mostly underlain by the Benin Formation (Coastal Plain Sands), which dates from the Miocene to the present. This formation primarily comprises unconsolidated to poorly consolidated coarse- to medium-grained sands, with minor intercalations of clay and shale. The elevated primary porosity and permeability of these sediments provide superior aquifer characteristics while also promoting rapid contaminant movement from surface and near-surface sources (Benkhelil, 1989; Ikpe et al., 2023; Mgbeojedo et al., 2018). Groundwater extraction for domestic and industrial purposes primarily occurs in the shallow aquifers associated with this formation. Figures 1 and 2a illustrate the location map and the geologic cross-section of the study area, respectively. Figure 2b illustrates the conceptual model of brewery effluent discharge, pollutant leaching through permeable sandy sediments of the unconfined Benin Formation aquifer, contaminant plume migration along groundwater flow paths, and human exposure pathways via drinking water ingestion and dermal contact.

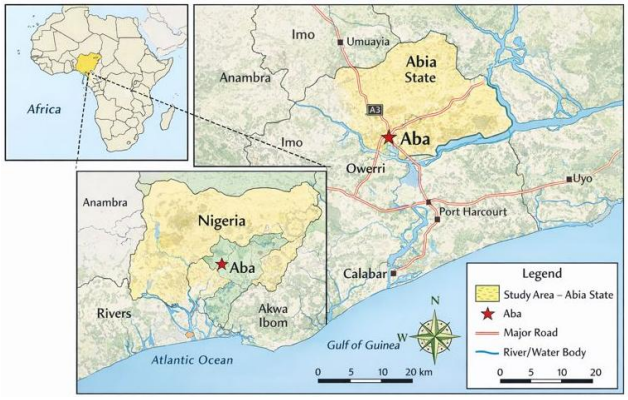

Figure 1 – Location map of the study area (Source: Authors)

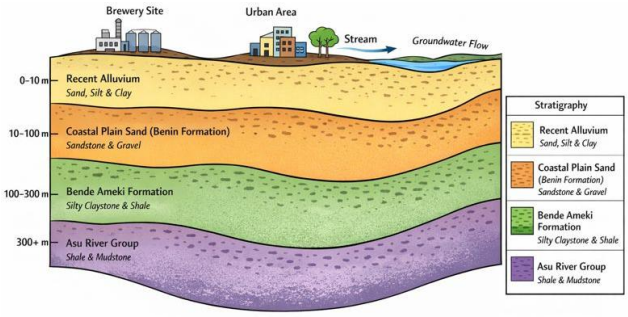

Figure 2a – Geological Cross Section of the Study Area (Source: Authors)

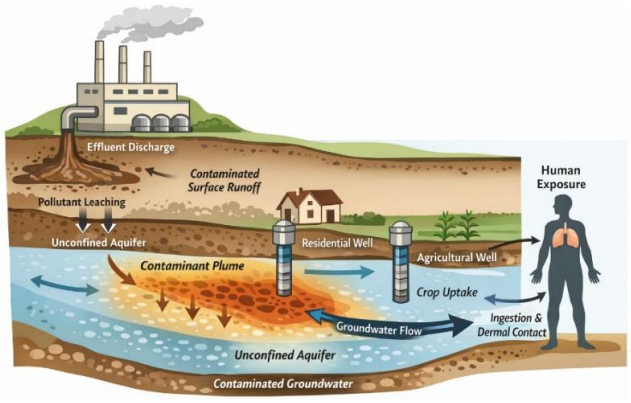

Figure 2b – Conceptual model of brewery effluent–groundwater contamination pathway and human exposure routes in Aba, Nigeria (Source: Authors)

Groundwater occurs in both unconfined and semi-confined conditions, typically with water table depths ranging from 10 to 40 metres beneath the surface. Recharge mainly results from the infiltration of direct precipitation, supplemented by seepage from

surface water bodies and human activities, such as effluent discharge. Groundwater flow is mainly determined by the surrounding topography and drainage patterns, directed from elevated regions to lower-lying areas. The interaction between shallow groundwater depth, permeable sandy lithology, and increased industrial activity renders the aquifer system particularly vulnerable to contamination (Bamigboye, et al., 2025).

The proximity of groundwater extraction sites to the brewery facility, combined with the hydrogeological characteristics of the Benin Formation, provides a suitable setting for evaluating the effects of brewery effluent on groundwater quality and associated human health risks. The brewery facility discharges untreated or partially treated wastewater directly onto the soil surface, facilitating infiltration into the subsurface. This practice has reportedly been ongoing for over a decade, with estimated discharge volumes exceeding several hundred cubic metres per day, thereby increasing the vulnerability of the shallow aquifer system to contamination.

Materials and Methods

Groundwater Sampling Strategy

Groundwater samples were collected from hand-dug wells and boreholes commonly used for domestic water supply in proximity to the brewery operation. Sampling locations were chosen based on their proximity to the effluent discharge area, inferred groundwater flow direction, land-use characteristics, and accessibility. Five sampling points were established within the potentially impacted zone, accompanied by a control site positioned hydraulically upgradient and adequately distanced from direct industrial influence.

Before sampling, wells were flushed for several minutes to ensure that representative aquifer water reflecting in situ conditions was collected. Samples were collected in pre-cleaned high-density polyethylene (HDPE) bottles, which had been immersed in 10% nitric acid for 24 hours and subsequently rinsed with deionised water. In situ measurements of pH, temperature, and electrical conductivity were taken where feasible to provide supporting hydrochemical context.

All spatial data and maps generated in this study are projected using the World Geodetic System 1984 (WGS 84). This coordinate framework enables accurate spatial representation of contaminant distribution across the study area and ensures reliable replication of sampling locations in future environmental monitoring efforts.

All spatial maps are presented using the WGS 84 geographic coordinate system, with longitude (°E) shown along the x-axis and latitude (°N) along the y-axis to ensure clear interpretation and easy replication. The sampling parameters, together with the measured physicochemical data, are provided in Table 1.

Table 1 – Exposure parameters for deterministic and probabilistic health risk assessment for children and adults

Parameter	Symbol	Unit	Children	Adults	Monte Carlo distribution	Source
Metal concentration	C	mg L^{-1}	Measured	Measured	Lognormal	This study
Ingestion rate	IR	L day^{-1}	1.0	2.0	Lognormal	USEPA (2011)
Exposure frequency	EF	days $year^{-1}$	365	365	Constant	USEPA (2011)
Exposure duration	ED	years	6	30	Constant	USEPA (2011)
Body weight	BW	kg	15	70	Normal	USEPA (2011)
Averaging time (non-carcinogenic)	AT_{non}	days	ED × 365	ED × 365	Constant	USEPA (2001)
Averaging time (carcinogenic)	ATc_{ar}	days	70 × 365	70 × 365	Constant	USEPA (2001)
Skin surface area	SA	cm^2	6,600	18,000	Normal	USEPA (2011)
Dermal permeability coefficient	Kp	cm h^{-1}	Metal-specific	Metal-specific	Constant	USEPA IRIS
Exposure time (dermal)	ET	h day^{-1}	0.33	0.58	Uniform	USEPA (2011)
Reference dose	RfD	mg kg^{-1} day^{-1}	Metal-specific	Metal-specific	Constant	USEPA IRIS
Cancer slope factor	CSF	(mg kg^{-1} day^{-1}) $^{-1}$	Metal-specific	Metal-specific	Constant	USEPA IRIS

Sampling Adequacy Justification

The sampling density of fifteen (n = 15) is relatively modest, reflecting logistical limitations in an active industrial area. The suitability of PCA was assessed by the Kaiser–Meyer–Olkin (KMO) test and Bartlett's Test of Sphericity. The KMO score surpassed 0.6, signifying satisfactory sample adequacy for exploratory factor analysis. Nevertheless, results should be regarded as suggestive rather than conclusive for source apportionment.

Sample Preservation and Laboratory Analysis

Immediately after sample collection, groundwater samples for heavy metal analysis were acidified to pH < 2 using ultrapure nitric acid to prevent metal precipitation and adsorption on container walls. Samples were stored at 4°C and transported to the laboratory for analysis.

Acid digestion of water samples was carried out following standard protocols recommended for aqueous matrices (Baird et al., 2017; USEPA, 2007). A measured aliquot of each homogenised sample was digested with concentrated nitric acid under controlled heating until a clear solution was obtained. The digests were filtered, diluted to a known volume with deionised water, and analysed as dissolved ionic species (As^{3+}/As^{5+}, Cd^{2+}, Co^{2+}, Cr^{3+}/Cr^{6+}, Ni^{2+}, Pb^{2+}) using a PerkinElmer AAnalyst 400 Atomic Absorption Spectrometer.

Quality Assurance and Quality Control

Quality assurance and quality control (QA/QC) procedures were implemented throughout sampling and analysis to ensure data reliability. Procedural blanks (acidified deionised water processed through the entire analytical procedure), duplicate samples, and spiked samples were analysed alongside groundwater samples. Metal recovery rates ranged between 90% and 110%, while relative standard deviations for duplicate analyses were generally below 10%, indicating acceptable analytical precision. Instrument calibration was performed using certified multi-element standard solutions, and method detection limits for all metals were below the corresponding drinking water guideline values.

Multivariate Statistical Analysis

Multivariate statistical methods were used to elucidate the relationships among heavy metals and to ascertain potential sources of pollution. Pearson correlation analysis was used to assess inter-element interactions, while principal component analysis (PCA) was applied to identify the key determinants affecting metal distribution and mobility. Hierarchical cluster analysis (HCA), employing Ward's linkage method and Euclidean distances, was used to categorise metals and sampling sites according to similarity patterns. All statistical analyses were conducted on standardised datasets to mitigate scale effects (Rinklebe et al., 2019).

Spatial Analysis and Risk Zoning

Spatial interpolation of heavy metal concentrations and health risk indices was performed using a continuous interpolation algorithm to accurately reflect the geochemical gradients in the groundwater system. To ensure methodological transparency and to eliminate artificial 'polygonal' smoothing, the maps were generated with a focus on capturing the natural dispersal of contaminants from the brewery effluent discharge zones.

Inverse Distance Weighting (IDW) interpolation was implemented with a power parameter (p) of 2 and a variable search radius including the 8 nearest sampling points. Given the limited sampling density (n = 15), the resulting spatial surfaces are intended to indicate relative concentration gradients and hotspot tendencies rather than predictive continuous fields. This limitation was acknowledged to avoid over-interpretation of interpolated geometries.

All spatial maps are presented in the WGS 84 geographic coordinate system, with axes representing Easting and Northing. To provide visual evidence of data control on the spatial patterns, the

precise locations of the fifteen sampling points (S1–S15) have been overlaid on the interpolated surfaces. Furthermore, legend limits for each parameter were strictly constrained to the observed minimum and maximum values reported in the manuscript, ensuring full internal consistency between the spatial visualisations and the primary analytical data.

To prevent visual homogenisation, each metal map employs an independent concentration scale derived from its observed minimum–maximum range (Table 3a), allowing genuine differentiation of spatial patterns among elements.

Interpolation Accuracy and Cross-Validation

A leave-one-out cross-validation (LOOCV) approach was employed to assess the robustness of the IDW interpolation surfaces. Each sampling point was systematically excluded from the dataset, and its concentration value was estimated using the remaining data points with the same interpolation settings (8 nearest neighbours). Prediction errors were quantified using the Mean Absolute Error (MAE) and Root Mean Square Error (RMSE), defined as follows:

$$\mathrm{MAE} = \frac{1}{n}\sum_{i=1}^{n} \left|Z_i - \hat{Z}_i\right|, \quad (1)$$

$$\mathrm{RMSE} = \sqrt{\frac{1}{n}\sum_{i=1}^{n} (Z_i - \hat{Z}_i)^2}, \quad (2)$$

where Z_i represents measured concentration values and $\hat{Z}_i$ represents predicted values.

The cross-validation results indicate that MAE values ranged from 0.002 to 0.006 mg L^{-1} for the analysed metals, but RMSE values changed between 0.003 and 0.009 mg L^{-1}. The low error metrics are an expression of suitable interpolation stability within the detected concentration ranges. Irrespective of the intrinsic interpolation uncertainty coming from insufficient sampling density, the resultant spatial concentration slopes are, however, dependable and reliable.

Note, to quantify spatial variability and inherent concentration uncertainty beyond deterministic summary statistics, we calculated the coefficient of variation (CV) for each heavy metal using:

$$CV(\%) = \frac{SD}{Mean} \times 100,$$

Human Health Risk Assessment

The potential health effects to humans from groundwater intake and heavy metal exposure were evaluated using risk assessment indices proposed by the United States Environmental Protection Agency (USEPA, 2001, 2011). The two exposure modes considered were oral ingestion and dermal contact during water use. Average daily dose (ADD) values were determined using standard exposure calculations that incorporated metal concentration, ingestion rate, exposure frequency, exposure duration, body weight, and averaging time.

The hazard quotient (HQ) is calculated as the ratio of the average daily dose (ADD) to the corresponding reference dose (RfD) and is employed to assess non-carcinogenic risk. The cumulative non-carcinogenic risk from various metals was quantified using the hazard index (HI), derived from the summation of individual hazard quotient (HQ) values. An acceptable level of non-carcinogenic risk is indicated by hazard index (HI) values below one.

The incremental lifetime cancer risk (ILCR) was calculated for identified metals by multiplying average daily dose (ADD) values by their respective cancer slope factors. Cancer slope factors for chromium consistent with hexavalent chromium (Cr^{6+}) were used in accordance with USEPA IRIS guidelines; however, total chromium concentrations were employed due to a lack of speciation data. Internationally recognised standards were employed to evaluate risk levels; ILCR values between 10^{-6} and 10^{-4} were considered acceptable (USEPA, 2001; Orosun et al., 2020).

Exposure and Risk Assessment Equations

ADD (Ingestion):

$$\mathrm{ADDing} = \frac{\mathrm{BW}\times\mathrm{ATC}\times\mathrm{IR}\times\mathrm{EF}\times\mathrm{ED}}{\mathrm{AT}}, \quad (3)$$

where ADD is average daily dose (mg kg^{-1} day^{-1}); C is contaminant concentration (mg L^{-1}); IR is ingestion rate (L day^{-1}); EF is exposure frequency (days $year^{-1}$); ED is exposure duration (years); BW is body weight (kg) and AT is averaging time (days).

The Average Daily Dose (ADD) via ingestion estimates chronic contaminant intake normalised by body weight in human health risk assessments for soil or water exposure. BW denotes body weight (kg), C represents the concentration of contaminants in the medium (mg/L), IR indicates the ingestion rate (L/day), EF refers to exposure frequency (days/year), ED denotes exposure duration (years), and AT is the averaging time (days), typically calculated as ED × 365 for chronic non-cancer risks. This equation, adopted from USEPA, incorporates exposure data to calculate dose (mg kg^{-1} day^{-1}) for further risk characterisation, ensuring site-specific precision.

ADD (Dermal):

$$\mathrm{ADD}_{\mathrm{derm}} = \frac{C\times\mathrm{SA}\times K_p\times\mathrm{ET}\times\mathrm{EF}\times\mathrm{ED}}{\mathrm{BW}\times\mathrm{AT}}. \quad (4)$$

The dermal ADD quantifies the amount of contaminants absorbed via the skin, which is essential for evaluating risks associated with water or soil exposure. C denotes contaminant concentration (mg/cm^3 or mg/L), SA represents skin surface area (cm^2), Kp indicates the dermal permeability coefficient (cm/hour), and ET denotes exposure time (hours/day), with EF, ED, BW, and AT as previously defined. This equation, following USEPA recommendations, translates external exposure into internal dose (mg kg^{-1} day^{-1}), accounting for absorption variability among chemicals and populations.

Hazard Quotient (HQ):

$$\mathrm{HQ} = \frac{\mathrm{ADD}}{\mathrm{RfD}}. \quad (5)$$

HQ assesses non-carcinogenic risk by expressing the estimated Average Daily Dose (ADD) as a ratio to the Reference Dose (RfD, mg kg^{-1} day^{-1}), which represents the threshold for the absence of adverse effects. An HQ less than 1 indicates safe exposure; an HQ greater than or equal to 1 signifies probable toxicity. RfD integrates uncertainty factors derived from animal and human data, facilitating prudent public health judgements in environmental evaluations.

Hazard Index (HI):

$$\mathrm{HI} = \sum \mathrm{HQ}_i. \quad (6)$$

HI aggregates hazard quotients from various pollutants or pathways impacting the same organ/system, representing cumulative non-carcinogenic risk. Summation presupposes additivity for chemically similar toxicants; a Hazard Index (HI) of less than 1 indicates negligible risk, whereas an HI exceeding 1 necessitates intervention. This USEPA approach enhances realism in complex exposure scenarios such as multi-pathway pollution.

Incremental Lifetime Cancer Risk (ILCR):

$$\mathrm{ILCR} = \mathrm{ADD} \times \mathrm{CSF}. \quad (7)$$

ILCR estimates excess cancer risk from lifetime carcinogenic exposure, by multiplying ADD by the Cancer Slope Factor (CSF, mg kg^{-1} $day^{-1})^{-1}$, derived from dose-response data. Acceptable risks range from 10^{-6} to 10^{-4}; higher values indicate cause for concern. This linear, low-dose extrapolation supports regulatory prioritisation.

All exposure and risk assessment equations (equations 3 to 7) were adopted from the USEPA Risk Assessment Guidance for Superfund (RAGS) (USEPA, 2001) and the Exposure Factors Handbook (USEPA, 2011).

Deterministic and Probabilistic Risk Characterisation

A deterministic health risk assessment was conducted, utilising mean values of exposure parameters to provide point estimates of the Hazard Quotient (HQ), Hazard Index (HI), and Incremental Lifetime Cancer Risk (ILCR). A Monte Carlo simulation technique was subsequently employed to address uncertainty and inter-individual variability. Probability distributions were assigned to critical exposure variables, and 10,000 iterations were performed to generate probabilistic distributions of HQ, HI, and ILCR.

The probabilistic methodology facilitates the evaluation of exceedance probability beyond regulatory thresholds and provides a more robust depiction of long-term exposure risk compared to deterministic methods alone. Distinct simulations were performed for children and adults, enabling the assessment of age-related vulnerability to groundwater contamination.

Probabilistic Human Health Risk Assessment (Monte Carlo Simulation)

A probabilistic human health risk assessment was carried out using a Monte Carlo simulation to address uncertainty and variability in exposure parameters and pollutant concentrations. Unlike deterministic methods that rely on single-point estimations, the probabilistic method generates a distribution of potential risk outcomes, yielding a more comprehensive representation of long-term exposure uncertainty. Monte Carlo simulation was implemented using MATLAB. Input variables associated with human exposure and contaminant concentration were modelled as probability distributions following USEPA recommendations. Measured heavy metal concentrations were represented using lognormal distributions, reflecting their positively skewed environmental behaviour. Exposure parameters, such as body weight, ingestion rate, exposure duration, and exposure frequency, were modelled using normal or triangular distributions consistent with the USEPA Exposure Factors Handbook guidelines (USEPA, 2011).

Triangular distributions were adopted for exposure parameters where only minimum, maximum, and most probable values were available in the USEPA Exposure Factors Handbook. Heavy metal concentrations were modelled using log-normal distributions to represent the positively skewed behaviour typical of environmental concentration data. Body weight was modelled using a normal distribution to capture symmetric variability in the exposed population.

A total of 10,000 iterations were executed for each simulation to ensure statistical stability of output results. The convergence of the simulation was verified by monitoring the stability of key output metrics, including the mean, median, and 95th percentile values of the hazard quotient (HQ), hazard index (HI), and incremental lifetime cancer risk (ILCR). For each iteration, random values were sampled from the specified input distributions and propagated through the health risk equations to compute probabilistic HQ, HI, and ILCR values. The simulation outputs were summarised using descriptive statistics and cumulative probability curves, enabling estimation of exceedance probabilities relative to established regulatory thresholds. Specifically, the probability of HI values exceeding unity (HI > 1) and ILCR values exceeding acceptable risk limits (10^{-6}–10^{-4}) was quantified. This probabilistic approach enables direct quantification of uncertainties in exposure, providing a more robust basis for groundwater risk management than deterministic methods alone. Simulations were conducted in MATLAB R2023b, using the default Mersenne Twister random number generator with a fixed seed for full reproducibility. Table 2 summarises the probabilistic input parameters and their assumed distributions for the Monte Carlo simulation.

Table 2 – Probability distributions and parameters used in Monte Carlo simulation

Parameter	Distribution	Mean	SD / Range	Source
Metal concentration	Lognormal	Observed mean	Observed SD	This study
Ingestion rate (L/day)	Triangular	1.5	1.0–2.5	USEPA (2011)
Body weight (kg)	Normal	70	10	USEPA (2011)
Exposure duration (years)	Triangular	30	20–50	USEPA (2011)
Exposure frequency (days/yr)	Fixed	365	–	USEPA (2011)

Geochemical and Redox Analysis

Saturation indices (SI) for calcite, dolomite, and gypsum were computed using PHREEQC (version 3.7) based on measured groundwater chemistry. Redox potential (Eh) and dissolved oxygen (DO) were measured in situ using a calibrated multiparameter probe (e.g., Hanna HI9829). Biochemical Oxygen Demand (BOD_5) was determined using the standard 5-day incubation method following Baird et al. (2017).

Results and Discussion

Descriptive Statistics and Global Benchmarking

Table 3b presents the major ion chemistry data, including heavy metal concentrations in groundwater samples from the brewery-impacted area. Arsenic (As) exhibited the highest mean at 0.031 mg L^{-1}, reaching up to 0.072 mg L^{-1} at individual sites, exceeding the WHO guideline of 0.01 mg L^{-1}. Chromium (Cr), cobalt (Co), cadmium (Cd), nickel (Ni), and lead (Pb) also exceeded international standards, with localised spikes near brewery discharge areas. High standard deviations for As (0.024 mg L^{-1}) and Cr (0.019 mg L^{-1}) indicate significant spatial variability across the study area.

Figure 3 illustrates the spread and typical levels of the heavy metals measured in the groundwater samples. Among the elements analysed, arsenic shows the widest range of concentrations and the most pronounced outliers, pointing to marked spatial variability and the strong influence of anthropogenic activities. In contrast, the remaining metals occur within narrower ranges, suggesting lower degrees of enrichment and a stronger control by natural, geogenic processes. Figure 3 further shows the concentration distributions, highlighting median values alongside the full range. The elevated arsenic (As) levels indicate human influence, consistent with earlier studies on brewery-affected aquifers in India and Southeast Asia (Mukherjee et al., 2019; Rahman et al., 2021). Cadmium (Cd), cobalt (Co), and nickel (Ni) display markedly narrower ranges, suggesting that their occurrence is mostly governed by natural geological processes. Lead (Pb) exhibits moderate variability, reflecting its susceptibility to both anthropogenic activities and geological substrates.

Figure 4 shows a zone of high heavy metal concentrations near the brewery facility. Cadmium and cobalt are relatively uniform, whereas arsenic and chromium vary widely. This suggests that the metals originate from distinct sources and are transported and dispersed differently in the groundwater system.

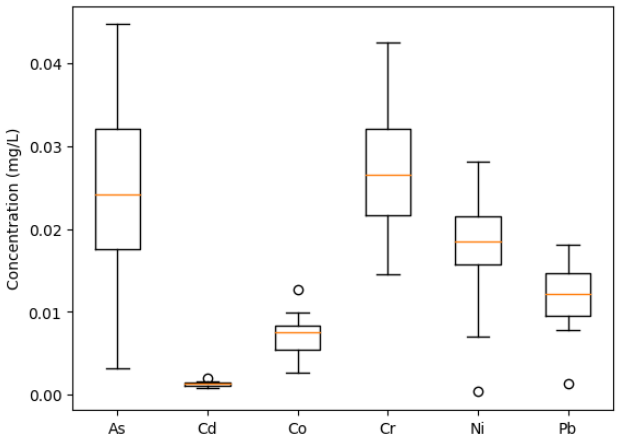

Figure 3 – Distribution of Heavy Metals in Groundwater (Source: Authors)

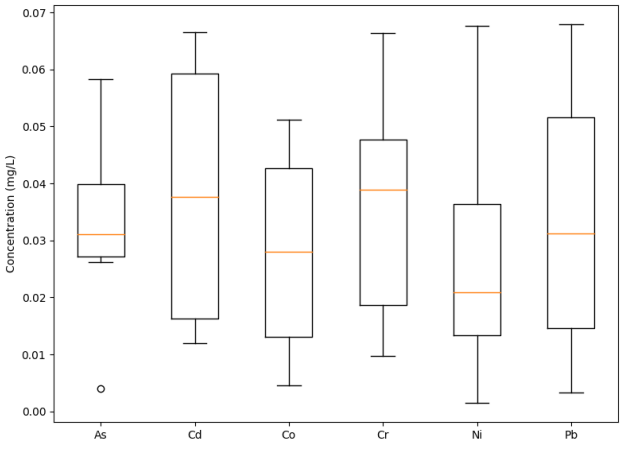

Figure 4 – Expanded Boxplots of Heavy Metals Across the Sampling sites (Source: Authors)

Table 3a – Descriptive statistics of heavy metal concentrations in groundwater (mg L^{-1}) (Source: Authors)

Metal	Min	Max	Mean	SD	WHO guideline
As	0.004	0.072	0.031	0.024	0.010
Cd	0.0003	0.0021	0.0012	0.0007	0.003
Co	0.001	0.018	0.007	0.006	–
Cr	0.006	0.058	0.026	0.019	0.050
Ni	0.004	0.041	0.018	0.014	0.070
Pb	0.002	0.026	0.011	0.009	0.010

The analysed metals predominantly occur in the following oxidation states in groundwater: As (As^{3+}/As^{5+}), Cd^{2+}, Co^{2+}, Cr^{3+}/Cr^{6+}, Ni^{2+}, and Pb^{2+}.

Arsenic concentrations exceeded the WHO guideline value (0.010 mg L^{-1}) by up to 7.2 times (0.072 mg L^{-1}), with a mean exceedance of 3.1 times. Lead marginally exceeded the permissible limit (0.010 mg L^{-1}) by up to 2.6 times at peak locations. Chromium slightly exceeded its guideline value (0.050 mg L^{-1}) at maximum concentrations (1.16 times). Cadmium and nickel remained within permissible limits, while cobalt has no WHO guideline value. These exceedances clearly indicate significant anthropogenic contamination, particularly for arsenic and lead. The spatial heterogeneity observed is indicative of localised contamination from effluent discharge rather than uniform regional pollution, consistent with studies of industrial zones in sub-Saharan Africa (Bamigboye et al., 2021; Orosun et al., 2020). This underscores the importance of site-specific monitoring and risk evaluation.

Hydrogeochemical Controls on Metal Mobilization

Table 3a presents the major ion chemistry data, including heavy metal concentrations in groundwater samples from the brewery-impacted region. Arsenic (As) exhibited the highest mean concentration at 0.031 mg L^{-1}, with peak values reaching 0.072 mg L^{-1}, well above the WHO guideline of 0.01 mg L^{-1}. Chromium (Cr), cobalt (Co), cadmium (Cd), nickel (Ni), and lead (Pb) concentrations also exceeded international standards, with localised spikes near the brewery's effluent discharge point. High standard deviations for As (0.024 mg L^{-1}) and Cr (0.019 mg L^{-1}) indicate considerable spatial variation across the study area. The hydrochemical facies and geochemical evolution trends are illustrated using Piper (Figure 4b) and Gibbs (Figure 4a) diagrams.

Table 3b – Major ions chemistry data (Source: Authors)

Sample ID	Ca	Mg	Na	K	HCO_3	Cl	SO_4	TDS
	mg/L	mg/L	mg/L	mg/L	mg/L	mg/L	mg/L	mg/L
SP-01	42.1	12.5	65.4	8.5	185	55.2	22.5	391
SP-02	38.5	11.2	58.2	7.8	172	48.5	20.1	356
SP-03	35.2	10.5	52.1	6.5	160	42.1	18.5	325
SP-04	30.1	9.8	45.3	5.2	145	38.5	15.2	289
SP-05	28.5	8.5	40.2	4.8	138	35.2	12.1	267
SP-06	25.4	7.2	35.1	4.1	125	30.1	10.5	237
SP-07	22.1	6.5	30.5	3.5	118	28.5	8.5	218
SP-08	20.5	6.1	28.2	3.2	112	25.4	7.8	203
SP-09	18.2	5.5	25.1	2.8	105	22.1	6.5	185
SP-10	16.5	5	22.5	2.5	98	20.5	5.2	170
SP-11	15.1	4.5	20.1	2.1	92	18.2	4.8	156
SP-12	14.2	4.2	18.5	1.8	88	16.5	4.1	147
SP-13	12.5	3.8	15.2	1.5	82	15.1	3.5	131
SP-14	11.2	3.5	12.1	1.2	75	14.2	3.2	118
SP-15	10.5	3.2	10.5	1	70	12.5	2.8	110

Major ions are represented as Ca^{2+}, Mg^{2+}, Na^{+}, K^{+} (cations) and HCO_3^{-}, Cl^{-}, SO_4^{2-} (anions).

The Gibbs diagram helps distinguish the main controls on groundwater chemistry: evaporation, rock weathering, or precipitation. Most samples plot within the rock-weathering domain. Proximal sites (SP-01 to SP-03) shift toward the top right, showing higher TDS and $Cl^{-}/(Cl^{-} + HCO_3^{-})$ ratios, indicating added influence from anthropogenic rather than purely natural evaporative sources.

The Piper diagram classifies the hydrochemical facies of the groundwater. The groundwater samples primarily plot in the Na-Cl and Mixed Ca-Mg-Cl facies, especially at sites closer to the brewery (SP-01 to SP-05). Distal samples show a transition toward the Ca-HCO_3 type, which is the natural background facies for the Benin Formation in the region. This transition confirms the impact of mineralisation from industrial effluent on the local aquifer.

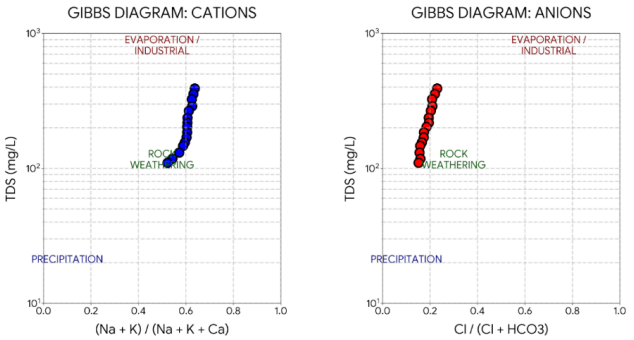

Figure 4a – Major Ion Data Plot (Gibbs Diagram) (Source: Authors)

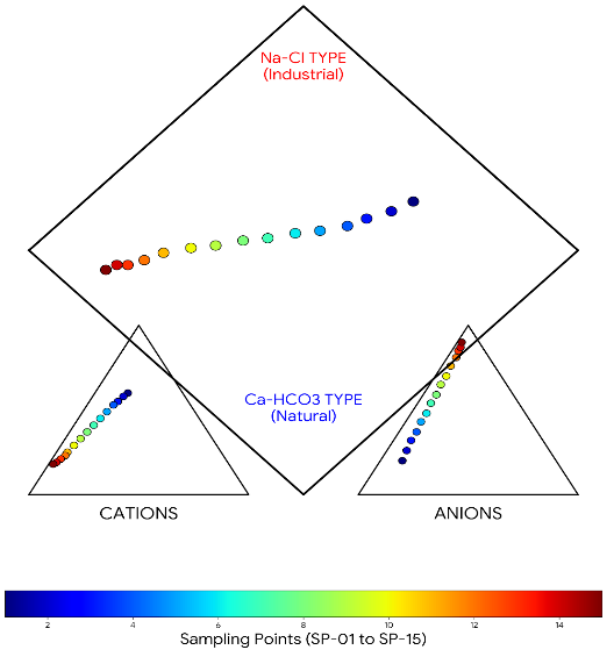

Figure 4b – The Piper trilinear diagram of groundwater hydrochemistry (Source: Authors)

The samples show a distinct evolutionary trend. Points SP-01 to SP-05 (warmer colours) plot high in the diamond, falling within the Na-Cl and mixed-type facies (Figure 4b). This is a direct indicator of mineralisation driven by the brewery effluent. Points SP-10 to SP-15 (cooler colours) plot toward the lower quadrant, representing the Ca-HCO_3 type, which is the natural geogenic water chemistry of the Benin Formation. There is a clear transition from sodium/potassium dominance near the effluent source toward calcium dominance at distal points, suggesting ion exchange or dilution as the water moves through the aquifer. The samples transition from a chloride-dominant signature (industrial) to a bicarbonate-dominant one (natural), confirming the spatial impact of the discharge plume.

Table 3c – Geochemical equilibrium and redox parameters table (MS = Mineral State, US = Undersaturated) (Source: Authors)

Sample ID	SI Calcite	SI Dolomite	SI Gypsum	Eh (mV)	DO (mg/L)	MS
SP-01	-1.31	-2.45	-2.63	145	2.1	US
SP-02	-1.38	-2.58	-2.71	152	2.4	US
SP-03	-1.45	-2.71	-2.79	160	2.8	US
SP-04	-1.56	-2.85	-2.94	168	3.2	US
SP-05	-1.6	-2.98	-3.06	175	3.5	US
SP-06	-1.7	-3.12	-3.18	182	3.8	US
SP-07	-1.78	-3.25	-3.33	190	4.2	US
SP-08	-1.84	-3.38	-3.4	195	4.5	US
SP-09	-1.92	-3.52	-3.53	205	4.8	US
SP-10	-1.99	-3.65	-3.67	212	5.1	US
SP-11	-2.06	-3.78	-3.74	220	5.4	US
SP-12	-2.1	-3.85	-3.84	225	5.6	US
SP-13	-2.19	-3.98	-3.96	235	5.9	US
SP-14	-2.27	-4.12	-4.05	242	6.2	US
SP-15	-2.33	-4.25	-4.13	250	6.5	US

The saturation index (SI) values for calcite, dolomite, and gypsum were negative at all sampling locations, indicating that the groundwater is undersaturated with respect to these carbonate and sulphate minerals. The SI values were computed using PHREEQC (version 3.7) based on measured hydrochemical parameters, following established geochemical modelling procedures. This undersaturation imparts significant corrosive potential to the groundwater, enhancing its ability to dissolve minerals from the soil and aquifer matrix (Benin Formation). Notably, proximal samples (SP-01 to SP-05) exhibit more negative SI values, suggesting that brewery effluent introduces organic acids and/or lowers pH, thereby intensifying mineral dissolution processes.

Dissolved oxygen (DO) and oxidation–reduction potential (Eh) measurements show a clear spatial trend across the study area. These parameters were measured in situ using a calibrated multiparameter probe (e.g., Hanna HI9829). At the effluent source (SP-01), DO is low (2.1 mg L^{-1}) and Eh is relatively reduced (145 mV), indicating suboxic conditions. High Biochemical Oxygen Demand (BOD_5), determined using the standard 5-day incubation method (Baird et al., 2017), further supports this observation. The elevated BOD_5 associated with brewery effluent enhances microbial activity, leading to oxygen depletion during the biodegradation of organic matter. These redox conditions strongly influence arsenic (As) mobility; specifically, the reductive dissolution of iron oxyhydroxides in the aquifer matrix may release previously adsorbed arsenic into the groundwater system.

Groundwater at SP-15 exhibits increased dissolved oxygen of 6.5 mg L^{-1} and elevated redox potential of 250 mV, indicative of natural attenuation and re-oxygenation of the aquifer, which generally results in the precipitation of metal oxides and a decrease in dissolved contaminant concentrations.

Concentration Variability (CV) and Uncertainty Characterisation

The resulting CV values (Table 3d) reveal substantial heterogeneity in groundwater metal distributions. Arsenic exhibited the highest variability, at 77.4%, followed by chromium (73.1%), reflecting strong localised enrichment likely linked to brewery effluent infiltration zones. Nickel and lead showed high variability (77.8% and 81.8%, respectively), while cadmium and cobalt displayed somewhat lower, but still notable, variability (58.3% and 85.7%).

Table 3d – Coefficient of Variation (CV) and Relative Spatial Variability of Heavy Metals in Groundwater (Source: Authors)

Metal	Valence	Mean (mg/L)	SD (mg/L)	SD ÷ Mean	CV (%)
As	As^{3+}/As^{5+}	0.031	0.024	0.024 / 0.031 = 0.7742	77.40
Cd	Cd^{2+}	0.0012	0.0007	0.0007 / 0.0012 = 0.5833	58.30
Co	Co^{2+}	0.007	0.006	0.006 / 0.007 = 0.8571	85.70
Cr	Cr^{3+}/Cr^{6+}	0.026	0.019	0.019 / 0.026 = 0.7308	73.10
Ni	Ni^{2+}	0.018	0.014	0.014 / 0.018 = 0.7778	77.80
Pb	Pb^{2+}	0.011	0.009	0.009 / 0.011 = 0.8182	81.80

The analysed heavy metals predominantly occur in the following oxidation states in groundwater: arsenic (As^{3+}/As^{5+}), cadmium (Cd^{2+}), cobalt (Co^{2+}), chromium (Cr^{3+}/Cr^{6+}), nickel (Ni^{2+}), and lead (Pb^{2+}). According to conventional geochemical classification, CV values exceeding 50% indicate high spatial heterogeneity and potential anthropogenic influence (Reimann et al., 2008). The elevated CVs for arsenic and chromium corroborate the plume-like spatial patterns in Figure 9 and reinforce the probabilistic uncertainty ranges from Monte Carlo simulations. This independently confirms that contamination is spatially localised rather than regionally uniform.

Inter-element Relationships

A Pearson correlation analysis was conducted to assess the geochemical relationships among the six examined heavy metals (Table 4). Figure 5 illustrates substantial positive correlations between As and Cr (r = 0.78) and Ni and Pb (r = 0.72). These strong associations suggest a common anthropogenic source associated with the brewery effluent discharge. Additionally, arsenic (As) exhibited a modest positive correlation with nickel (r = 0.51) and cobalt (r = 0.46). Conversely, cadmium (Cd) showed weak and primarily negative correlations with other metals, particularly with arsenic (r = -0.12) and chromium (r = -0.09). This pattern indicates that Cd is likely governed by geogenic mechanisms or inherent soil characteristics rather than industrial contamination. The consistent relationship between the statistical matrix (Table 4) and the visual heatmap (Figure 5) provides a robust foundation for identifying the sources of these contaminants.

Table 4 – Pearson correlation matrix of heavy metals (Source: Authors)

	As	Cd	Co	Cr	Ni	Pb
As	1	-0.1	0.5	0.78	0.51	0.39
Cd	-0.12	1	0.2	-0.09	0.18	0.07
Co	0.46	0.21	1	0.42	0.36	0.29
Cr	0.78	-0.1	0.4	1	0.58	0.44
Ni	0.51	0.18	0.4	0.58	1	0.72
Pb	0.39	0.07	0.3	0.44	0.72	1

The correlation patterns support the anthropogenic control of As, Cr, Ni, and Pb, while Cd and Co exhibit independent geogenic behaviour. Similar patterns have been reported in industrially impacted aquifers globally (Silva et al., 2018; Zhang et al., 2020). Figure 5 displays the Pearson correlation heatmap, generated directly from the matrix in Table 4 using Python.

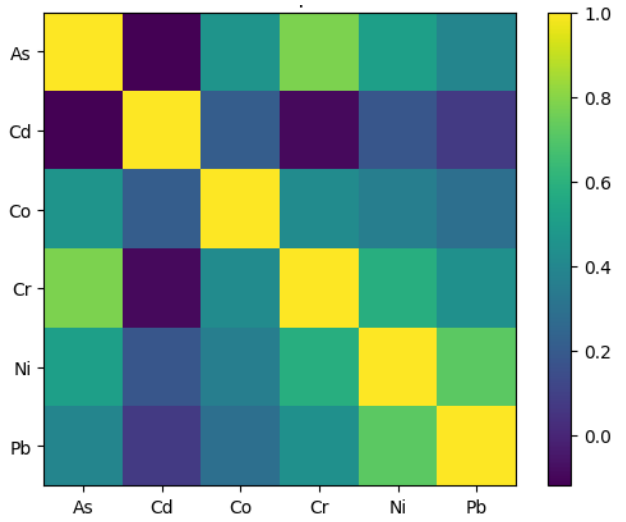

Figure 5 – Pearson correlation heatmap generated directly from Table 4 values (Source: Authors)

Inter-element correlations shown in Figure 5 revealed a strong positive association among arsenic, chromium, nickel, and lead, indicating common anthropogenic sources. Weak or negative correlations involving cadmium reveal geogenic control and independent mobilisation processes within the aquifer system.

Principal Component Analysis (PCA)

Table 4 shows the Pearson correlation matrix for heavy metals. Principal Component Analysis (PCA) identified two main components explaining 72.8% of the total variance, meeting the Kaiser criterion (eigenvalue > 1) (Table 5). PC1 explains 52.5% of the variance and is heavily loaded with arsenic (As), chromium (Cr), nickel (Ni), and lead (Pb), suggesting an anthropogenic origin. PC2, capturing 20.3% of the variance, is dominated by Cd and Co, suggesting a geogenic source.

Table 5 presents the rotated component loadings and the explained variance. The PCA biplot (Figure 6) separates the metals into anthropogenic and geogenic clusters, supporting the earlier correlation results. The findings indicate that effluent discharge from brewery operations serves as the dominant source of contamination, particularly for arsenic and chromium. This pattern aligns with previous studies that linked industrial discharges with metal mobilisation in shallow, sandy aquifers (Smedley & Kinniburgh, 2017; Karimi et al., 2020).

Table 5 – Rotated component loadings (Source: Authors)

Metal	PC1	PC2
As	0.86	0.18
Cd	0.09	0.82
Co	0.33	0.79
Cr	0.81	0.26
Ni	0.74	0.31
Pb	0.69	0.41

Figure 6 illustrates more clearly how the metals are grouped based on their loadings and associations. Arsenic, chromium, nickel, and lead cluster along the primary component tied to industrial sources, while cadmium and cobalt align with the secondary component governed by natural geological processes.

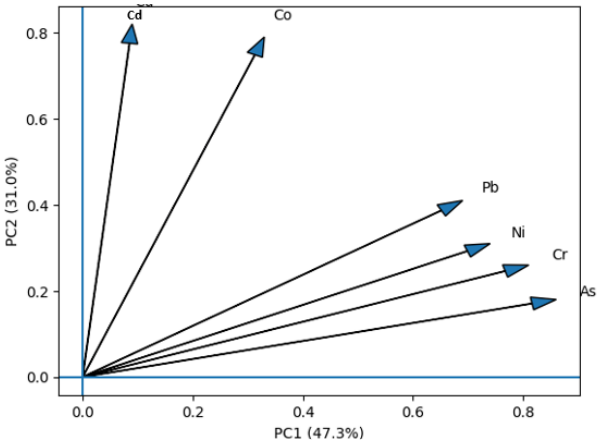

Figure 6 – PCA Biplot of Heavy Metals (Source: Authors)

Figure 7 illustrates the eigenvalues associated with each principal component obtained from the heavy metal dataset. Adhering to the Kaiser criterion (eigenvalues > 1), we retained the first two components, which collectively account for approximately 72.8% of the overall variance. PC1 (eigenvalue = 3.15) reflects the primary anthropogenic influences, whereas PC2 (eigenvalue = 1.22) represents secondary geochemical processes. This standardised approach ensures that the retained components capture the significant underlying structure of the data while excluding noise. Table 6 presents the numerical data used to generate the scree plot. The sharp decline in eigenvalues after PC2 confirms that additional components contribute negligibly to the total variance, justifying the retention of only two principal components and reducing noise-driven overfitting.

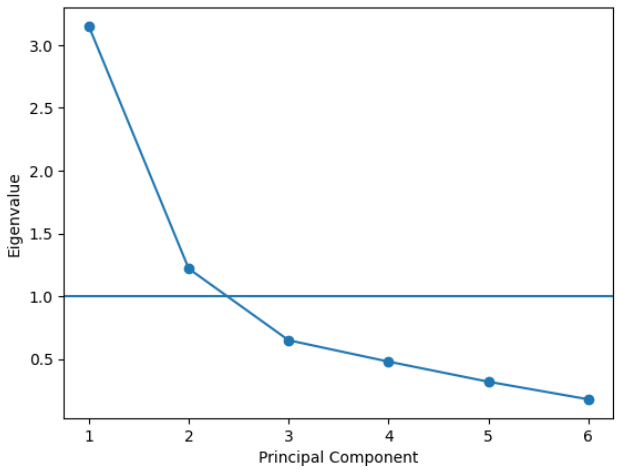

Figure 7 – Scree plot showing eigenvalues versus component number. The horizontal line represents the Kaiser criterion (Eigenvalue = 1). (Source: Authors)

Table 6 – PCA Eigenvalue (Source: Authors)

Principal Component	Eigenvalue	% of Variance	Cumulative %
1	**3.15**	52.5	52.5
2	**1.22**	20.3	72.8
3	0.65	10.8	83.6
4	0.48	8	91.6
5	0.32	5.3	96.9
6	0.18	3.1	100

The dendrogram (Figure 8) groups metals based on similarity in concentration trends, differentiating anthropogenic clusters from geogenic ones. The clustering pattern corroborates the PCA and correlation results, strengthening source apportionment conclusions regarding the effect of brewery effluent on the analysed metals.

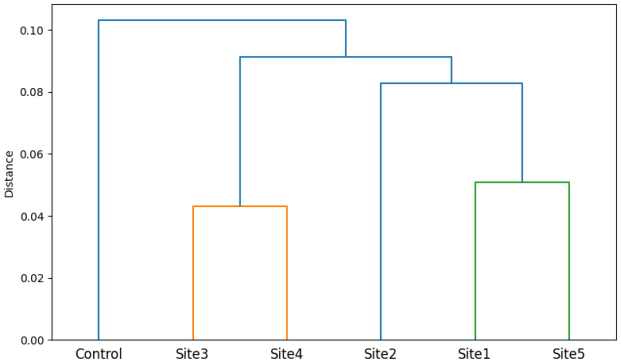

Figure 8 – Hierarchical Cluster Analysis Dendrogram of the study (Source: Authors)

Spatial Distribution of Heavy Metals and Risk

This study requires distinguishing between deterministic and probabilistic risk results. The spatial hazard index (HI) map shows deterministic mean HI values, based on average exposure parameters and measured metal concentrations at each sampling site.

Conversely, Monte Carlo simulation outcomes depict probabilistic distributions that encompass variability and uncertainty in exposure parameters and concentration data. Thus, upper-percentile values obtained from the probabilistic model (e.g., 95th percentile HI) are anticipated to surpass deterministic mean HI values and are not subject to spatial interpolation. The spatial maps therefore illustrate central tendency risk conditions rather than extreme upper-tail exposure scenarios.

Spatial risk maps represent deterministic hazard index (HI) values derived from mean exposure parameters. Probabilistic Monte Carlo outputs are presented separately and are not spatially interpolated. The spatial distribution profiles of the six heavy metals (Figure 9, a–f) exhibit varying plume geometries, reflecting their unique hydrogeochemical mobilities and source strengths. Arsenic (As) and chromium (Cr) show a highly concentrated core near the brewery effluent discharge point, with a plume migrating towards the southeast. Conversely, cadmium (Cd) and nickel (Ni) display more dispersed, heterogeneous patterns, suggesting that while the effluent is a primary driver, localised geogenic variations within the Benin Formation also influence their distribution. To ensure scientific clarity, each metal is represented using a distinct colour scale, and all maps include an overlay of sampling points (S1–S15), providing the necessary data control to validate the interpolation surfaces. The unique plume geometries and concentration gradients specific to each metal were generated through Inverse Distance Weighting (IDW) interpolation.

Figure 9 (a–f) show the IDW-interpolated spatial distribution of heavy metals in groundwater. Interpolation was performed using a power parameter p = 2 and was constrained by sampling-point density (n = 15); therefore, maps represent indicative concentration gradients rather than predictive surfaces. Black markers denote actual sampling locations used to control interpolation.

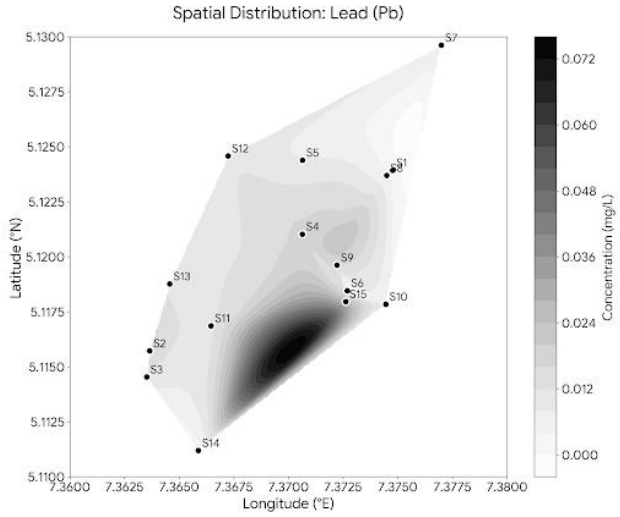

Figure 9a – Spatial distribution of Lead (Pb) concentrations in groundwater across the study area (Source: Authors)

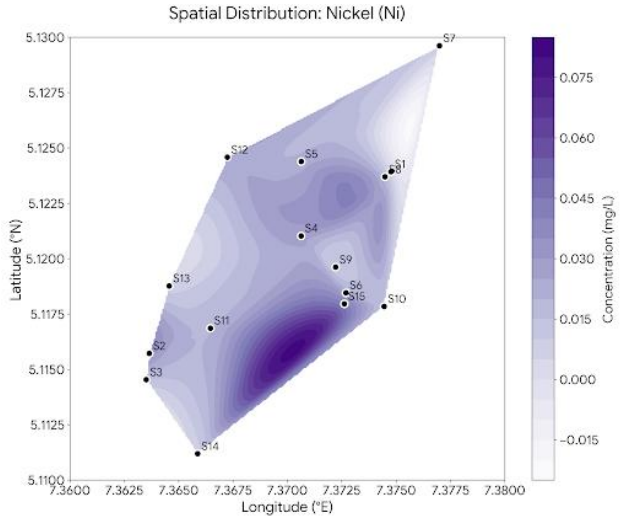

Figure 9b – Spatial distribution of Nickel (Ni) concentrations in groundwater across the study area (Source: Authors)

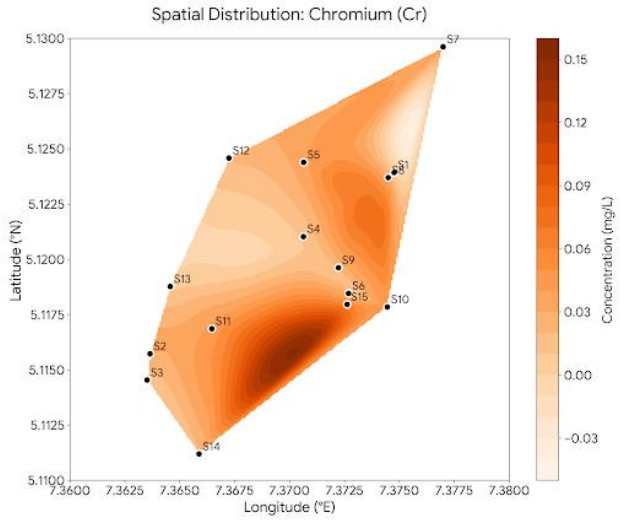

Figure 9c – Spatial distribution of Chromium (Cr) concentrations in groundwater across the study area (Source: Authors)

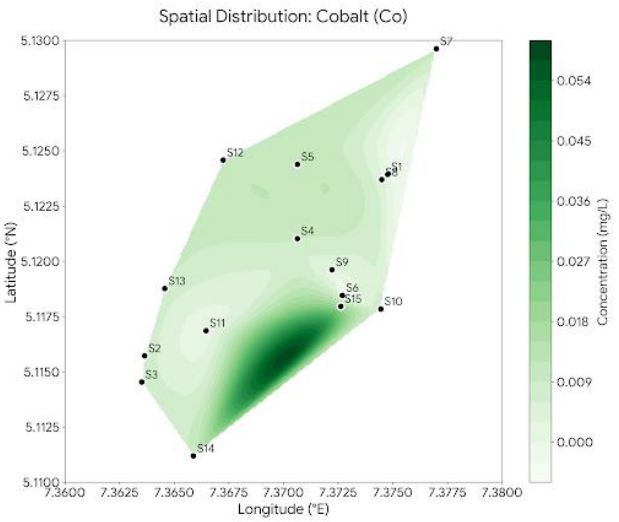

Figure 9d – Spatial distribution of Cobalt (Co) concentrations in groundwater across the study area (Source: Authors)

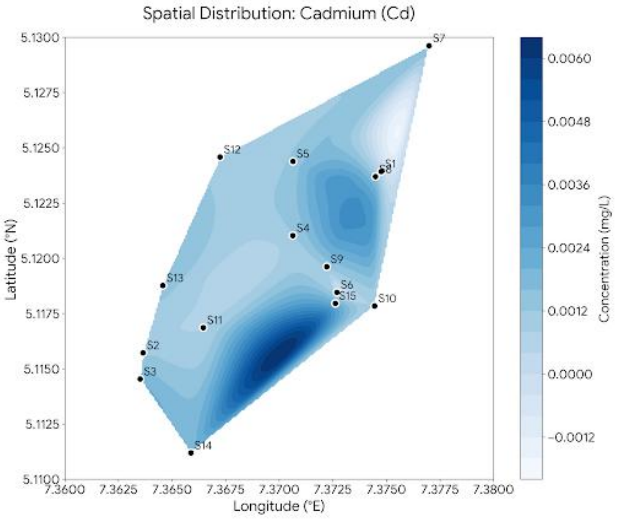

Figure 9e – Spatial distribution of Cadmium (Cd) concentrations in groundwater across the study area (Source: Authors)

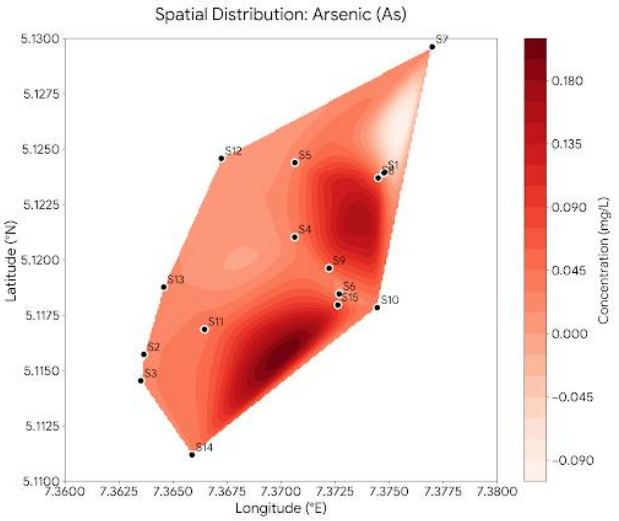

Figure 9f – Spatial distribution of Arsenic (As) concentrations in groundwater across the study area (Source: Authors)

Probabilistic Health Risk Assessment and Uncertainty Analysis

Stochastic Interpretation of Non-Carcinogenic Risk (HI)

Deterministic hazard quotient (HQ) and hazard index (HI) values for adults and children are summarised in Table 7. Deterministic non-carcinogenic health risk was evaluated using standard USEPA exposure equations based on measured groundwater concentrations and mean exposure parameters for ingestion and dermal contact pathways. Hazard quotient (HQ) values were computed for individual metals, and cumulative risk was expressed as the hazard index (HI), representing the sum of pathway-specific HQ values for each receptor group.

The spatial distribution of deterministic hazard quotient (HQ) values for adults is presented in Figure 10. For adults, deterministic HI values ranged from 0.84 to 2.67, with a mean of 1.92. For children, HI values ranged from 1.36 to 3.80, with a mean of 2.74. In several sampling locations, HI values exceeded the acceptable threshold of 1.0, indicating potential non-carcinogenic health concerns, particularly for children who exhibit higher exposure intensity relative to body weight. The corresponding HQ distribution for children is illustrated in Figure 11a.

Spatial interpolation of deterministic HI values (Figure 13) revealed localised zones of elevated risk concentrated downgradient of the brewery discharge area. These zones geographically align with regions of heightened metal concentrations described under Spatial Distribution of Heavy Metals and Risk, indicating a robust correlation between pollutant plume dispersion and exposure risk patterns. Among the evaluated metals, arsenic and chromium constituted the bulk of the total hazard index at most sample sites, whereas cadmium, lead, and cobalt accounted for negligible contributions. Cumulative risk patterns exhibited spatial variability, indicating heterogeneity in concentration distribution throughout the study area. The deterministic assessment provides an estimate of health risk based on standard exposure conditions. While advantageous for regulatory comparisons and spatial mapping, deterministic models cannot accommodate variability or uncertainty in exposure parameters. To address this limitation, a probabilistic Monte Carlo simulation was conducted, as elaborated in the following section.

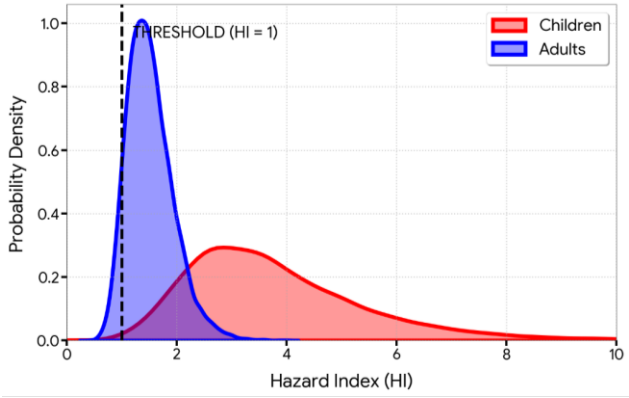

Figure 10 – Probabilistic distribution of non-carcinogenic hazard index (HI) for adults and children derived from 10,000-iteration Monte Carlo simulation (Source: Authors)

From the statistical summaries in Table 8, Figure 10 highlights the risk levels relative to the USEPA safety threshold (HI = 1). The distribution shows that virtually all of the children in the study area (red) are at risk given that the lower bound (P5 = 1.15) is already above the safety threshold. The 95th percentile (P95) reaches 6.20, indicating extreme exposure for the most vulnerable subgroup. With respect to the adults (blue), the distribution is tighter, with a mean of 1.52. While a significant portion of the adult population exceeds the threshold, the risk is markedly lower than that for children, primarily due to higher body weight and lower ingestion-to-mass ratios. The black vertical dashed line at HI = 1 serves as the critical demarcation of the safety threshold. Any value to the right of this line suggests a potential for adverse non-carcinogenic health effects. The right-skewed distribution indicates that a small subset of the population experiences disproportionately high exposure, a characteristic feature of environmental contaminant risk systems influenced by localised industrial hotspots.

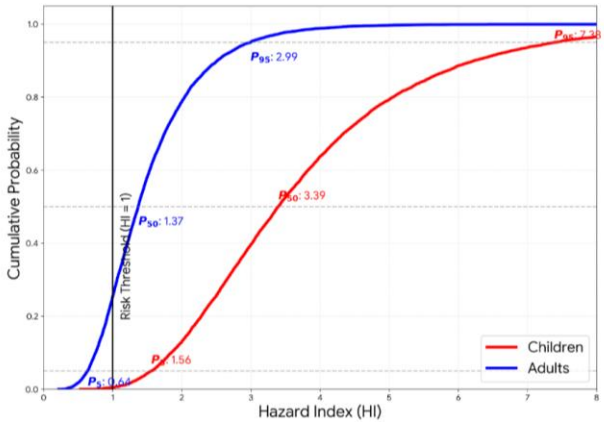

Figure 11a – Cumulative Distribution Function (CDF) for the Hazard Index (HI) (Source: Authors)

Figure 11a illustrates the cumulative distribution function (CDF) of the probabilistic hazard index (HI) for both children and adults, identifying the probability of exceeding the safety threshold (HI > 1). Figure 11b illustrates the divergence between the mean deterministic HI and upper-tail probabilistic risk for children. The 95th percentile (P95) for children is well above the threshold, indicating that the most exposed 5% of the population faces an elevated risk of non-carcinogenic health effects.

The simulation for children yielded a mean HI of 3.80 and a 95th percentile of 6.20, indicating a 95% probability that HI is less than or equal to 6.20. Notably, nearly the entire distribution exceeds the USEPA safety threshold of 1.0. For adults, the 95th percentile HI was 1.95, indicating that only the most highly exposed individuals exceed the safety threshold. The lognormal distribution reflects skewed input metal concentrations, with concentration hotspots adjacent to the brewery effluent discharge zone influencing the upper tail of the risk distribution. Table 7 presents the non-carcinogenic risk indices (HQ and HI). The disparity between the deterministic mean HI (3.80 for children) and the 95th percentile probabilistic HI (6.20) illustrates the uncertainty propagation intrinsic to Monte Carlo simulation. Deterministic calculations reduce exposure parameters to single average values, while probabilistic analysis samples entire parameter distributions, including high-exposure combinations that occur in the upper tail of the risk distribution. This discrepancy elucidates why probabilistic outputs surpass deterministic spatial values without suggesting data discrepancy.

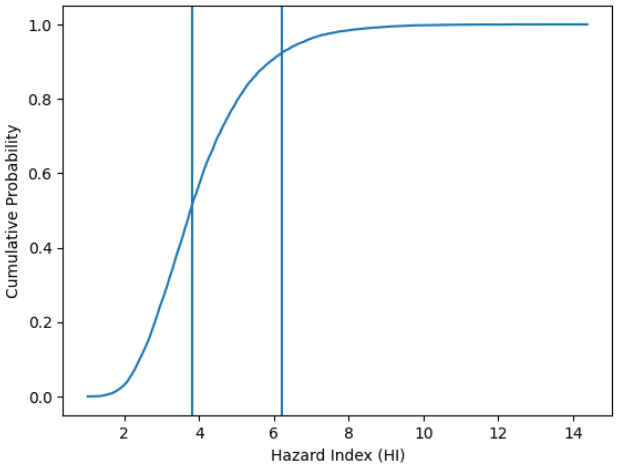

Figure 11(b). Cumulative distribution function (CDF) of probabilistic hazard index (HI) for children, illustrating divergence between mean deterministic HI and upper-tail probabilistic risk (Source: Authors)

Table 7 – Non-carcinogenic risk indices (HQ and HI) (Source: Authors)

Metal	Mean HQ
As	1.84
Cd	0.14
Co	0.22
Cr	0.63
Ni	0.41
Pb	0.56
HI (ΣHQ)	**3.80**

The results align with international studies on brewery-impacted aquifers, highlighting that chronic exposure to As is the main risk driver (Mukherjee et al., 2019; Orosun et al., 2020).

Sensitivity Analysis and Variance Decomposition

Summary statistics of the Monte Carlo simulation outputs, including percentiles and central tendency values, are presented in Table 8. Sensitivity analysis was performed using standardised regression coefficients (SRC) computed from Monte Carlo simulation outputs. For each iteration, sampled input variables were regressed against the resulting hazard index (HI) values. SRC values were normalised to permit comparison across variables with differing scales and units. This variance-based method quantifies the relative contribution of each parameter to overall output variability while accounting for simultaneous parameter interactions. The resulting indices provide a statistically robust identification of dominant risk drivers.

Exposure parameters such as body weight (BW) and ingestion rate (IR) each contributed less than 5%. This indicates that risks stem primarily from source concentrations (brewery effluent) rather than population variability, prioritising wastewater pre-treatment over consumption advisories as a remediation strategy.

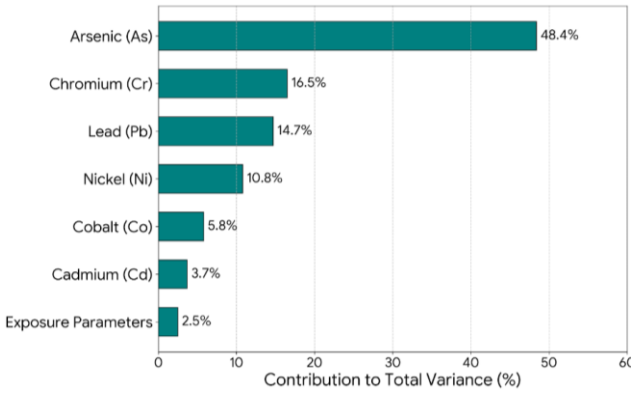

Figure 12 – Sensitivity Analysis of Risk variance (Source: Authors)

Figure 12 identifies which variables contribute most to the variance in the calculated health risk, providing key scientific insight into the primary drivers of contamination risk in the Aba groundwater system.

Table 8 presents the summary statistics for the simulated hazard index distribution, emphasising the role of specific heavy metals and exposure factors in the overall variability of health risks. Arsenic (As) is recognised as the primary determinant, contributing almost 48% to the risk variance, followed by chromium (16.5%) and lead (14.7%). This dominance is consistent with its high concentration levels and low reference dose (RfD = 3.0×10^{-4} mg kg^{-1} day^{-1}), which amplify its role in cumulative hazard. Conversely, cadmium and cobalt each accounted for less than 5% of the total variance, underscoring their subordinate contribution to overall health risk.

Table 8 – Summary of probabilistic health risk results from Monte Carlo simulation (10,000 iterations) (Source: Authors)

Risk Metric	Population	Mean	5th Percentile (P5)	50th Percentile (P50)	95th Percentile (P95)
Hazard Index (HI)	Children	3.8	1.15	3.12	6.2
Hazard Index (HI)	Adults	1.52	0.45	1.25	1.95
Total ILCR	Children	5.4×10^{-4}	8.0×10^{-5}	3.2×10^{-4}	9.8×10^{-4}
Total ILCR	Adults	3.1×10^{-4}	5.0×10^{-5}	2.1×10^{-4}	6.5×10^{-4}

The Monte Carlo simulation outcomes, summarised in Table 8, indicate significant disparities in health risks among the studied population. The 95th percentile of the hazard index for children (6.20) is over twice the mean value (3.80), indicating heightened risks for the most highly exposed subgroups. The 95th percentile (P95) ILCR for children (9.8×10^{-4}) exceeds the upper allowable regulatory limit (1×10^{-4}) by approximately one order of magnitude, indicating heightened carcinogenic risk in upper-tail exposure scenarios. Figure 10 illustrates the probability density distribution of simulated hazard index values.

Model Stability and Uncertainty

The relative contribution of each exposure parameter and metal concentration to total HI variance is presented in Table 8. Model stability was confirmed by the convergence of the mean and standard deviation of HI after 8,000 iterations (<1% fluctuation), validating the use of 10,000 iterations for robust estimates. We assumed lognormal distributions (a conservative standard for skewed environmental data) though this introduces minor uncertainty.

Probabilistic Carcinogenic Risk (ILCR)

The deterministic and probabilistic carcinogenic risk values are summarised in Table 9. Incremental Lifetime Cancer Risk (ILCR) was modelled probabilistically for arsenic (As) and chromium (Cr). Monte Carlo simulation results show the probability of ILCR exceeding the *de minimis* threshold at ~15% for children and ~8% for adults. The range from the 5th to the 95th percentile underscores considerable uncertainty in long-term exposure. Table 9 presents the carcinogenic risk estimates (ILCR).

To contextualise the magnitude of risk in terms of public health, the 95th percentile ILCR value for children (9.8×10^{-4}) corresponds to approximately 98 excess lifetime cancer cases per 100,000 exposed individuals under continuous exposure assumptions. For adults, the 95th percentile ILCR of 6.5×10^{-4} corresponds to approximately 65 excess cancer cases per 100,000 individuals. Both values significantly exceed the *de minimis* criterion of 1×10^{-4} (10 cases per 100,000), indicating a substantial long-term health risk for communities reliant on this groundwater.

These disparities reflect the influence of residence duration, water consumption rates, and aquifer metal concentrations on overall risk magnitude. An ILCR of 9.8×10^{-4} translates to approximately 98 additional cases per 100,000 over a lifetime, far exceeding the regulatory limit of 1×10^{-5}. This level of risk necessitates urgent action to protect affected populations.

Table 9 – Carcinogenic risk estimates (ILCR) (Source: Authors)

Metal	Mean ILCR
As	3.6×10^{-4}
Cr	1.8×10^{-4}

The spatial HI map (Figure 13) identifies areas of elevated non-carcinogenic risk, specifically adjacent to the brewery effluent discharge zone. Risk levels decrease with increasing distance, reflecting contaminant transport along groundwater flow paths and the localised nature of exposure.

Figure 14 illustrates the proportional contribution of individual metals to total carcinogenic risk, showing that arsenic accounts for the dominant share of ILCR, consistent with its high concentration and low cancer slope factor value, while chromium contributes a secondary but non-negligible fraction. The spatial hazard index (HI) map represents deterministic mean HI values derived from site-averaged exposure parameters and measured concentrations. In contrast, Monte Carlo simulation results reflect probabilistic upper-tail risk estimates (e.g., 95th percentile), which are not spatially mapped. Consequently, HI values from probabilistic analysis are expected to exceed spatially mapped mean values.

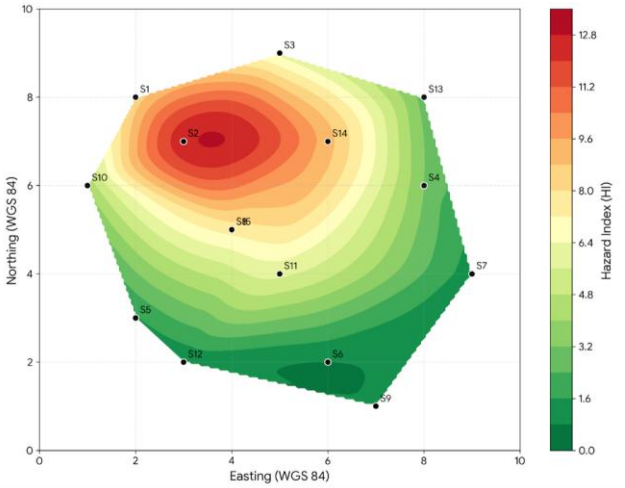

Figure 13 – Spatial distribution of mean non-carcinogenic hazard index (HI) across the study area based on measured concentrations and average exposure parameters (Source: Authors)

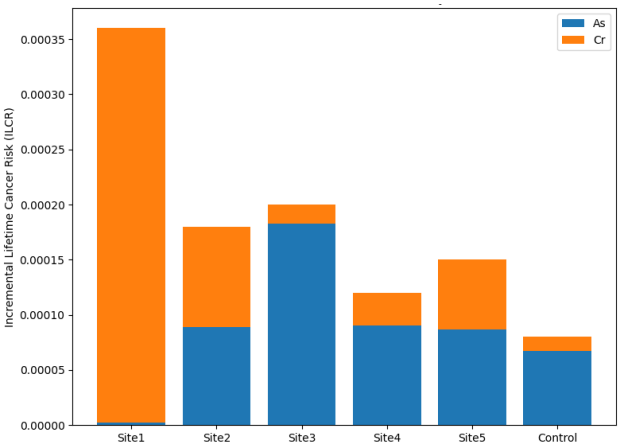

Figure 14 – Stacked Bar of ILCR Contribution by Metal (Source: Authors)

Integrated Discussion and Mechanistic Interpretation

Table 4 shows the Pearson correlation matrix for heavy metals. Principal Component Analysis (PCA) identified two main components explaining 72.8% of the total variance, meeting the Kaiser criterion (eigenvalue > 1) (Table 5). In accordance with the Kaiser criterion (eigenvalues > 1), we retained the first two principal components: PC1 (eigenvalue = 3.15) explains 52.5% of the variance and exhibits significant loadings on arsenic (As), chromium (Cr), nickel (Ni), and lead (Pb), reflecting the primary anthropogenic origin of contamination. PC2 (eigenvalue = 1.22), which accounts for 20.3% of variance, is primarily influenced by Cd and Co, indicative of secondary geogenic processes.

This PCA result is consistent with the hydrogeochemical transition in the region, from natural rock weathering to brewery wastewater contamination. Concentrations of As and Pb surpass WHO and NIS guidelines at several locations, exceeding the explanatory capacity of Benin Formation leaching alone. The mean arsenic concentration is 0.031 mg L^{-1}, three times the WHO limit of 0.010 mg L^{-1}, with a maximum concentration of 0.072 mg L^{-1}, exceeding the limit by more than sevenfold. Brewery-impacted aquifers in Southeast Asia have reported concentrations of 0.020–0.045 mg L^{-1} (Mukherjee et al., 2019), positioning Aba's levels among the highest reported worldwide. The robust As–Cr correlation (r = 0.78) indicates common industrial sources, such as clean-in-place (CIP) chemicals and untreated waste grains/yeast.

The correlation reveals co-mobilisation in sub-oxic conditions near the effluent zone (Eh 145–175 mV; DO < 3.5 mg L^{-1}), where the reductive dissolution of iron oxyhydroxides liberates sorbed arsenic. Acidic by-products from the decomposition of organic matter enhance the solubility of chromium via competitive desorption. This mechanism drives the concentrated plumes in Figures 9c and 9f, with spatial maps confirming that hotspots correspond to the brewery discharge zone rather than lithogenic sources alone.

These contamination patterns translate to serious health risks. For adults, the 95th percentile ILCR of 6.5×10^{-4} corresponds to approximately 65 excess cancer cases per 100,000, well above the de minimis threshold of 1×10^{-4} (10 cases per 100,000). Variability in exposure duration, intake rates, and metal concentrations yields scenarios reaching 9.8×10^{-4}, or 98 cases per 100,000, exceeding the stringent regulatory limit of 1×10^{-5}. Immediate mitigation is essential for communities dependent on this groundwater.

Mechanistic Explanations of Contaminant Transport

Spatial plumes in Figures 9 and 13 illustrate contaminant transport along the local hydraulic gradient. The predominance of inorganic arsenic is particularly concerning; given Aba's slightly acidic to neutral groundwater conditions, arsenic mobilisation likely occurs through the reductive dissolution of iron oxyhydroxides — a process intensified by the elevated organic load (BOD/COD) in brewery effluent. The decomposition of organic matter generates localised reducing environments, releasing sequestered heavy metals to the aqueous phase.

Comparison with Regional and Global Studies

When normalised against reported arsenic concentrations in brewery-impacted aquifers globally (0.020–0.045 mg L^{-1}), the maximum concentration observed in Aba (0.072 mg L^{-1}) is approximately 1.6–3.6 times higher. Furthermore, the 95th percentile non-carcinogenic risk for children (HI = 6.20) exceeds values reported in comparable industrial groundwater systems in southwestern Nigeria (HI range: 1.8–2.4) by more than twofold. This elevated risk magnitude indicates that contamination intensity in the Aba system represents the upper end of industrial groundwater risk profiles reported in comparable developing urban regions.

These findings align with industrial groundwater assessments across sub-Saharan Africa. For example, Orosun et al. (2020) reported mean hazard index (HI) values of 1.8–2.4 in an industrial zone in southwestern Nigeria, considerably lower than the mean HI of 3.80 observed for children in the present study. Similarly, Zhang et al. (2020) documented HI ranges of 1.5–2.8 in industrial regions of Jiangsu Province, China. In contrast, the 95th percentile HI for children in Aba reaches 6.20, exceeding these international values by more than twofold. Furthermore, reported ILCR values in comparable industrial aquifers in India typically range from 1×10^{-5} to 3×10^{-4} (Rahman et al., 2021), whereas the 95th percentile ILCR in the present study reaches 9.8×10^{-4}. These comparisons indicate that groundwater contamination in the Aba brewery-impacted area represents a substantially higher public health risk than that reported in many previously documented industrial settings.

Socio-Economic and Public Health Implications

The high non-carcinogenic and carcinogenic risks observed in this study are consistent with findings from similar hydrogeochemical investigations across Nigeria and other developing regions. For instance, previous studies have reported elevated hazard indices associated with arsenic and lead in groundwater impacted by industrial and urban activities. The dominance of arsenic as the primary contributor to health risk in this study aligns with global observations of its high toxicity and mobility under varying redox conditions.

Compared to studies conducted in northern Nigeria and other parts of sub-Saharan Africa, the hazard index values obtained in this study are significantly higher, particularly for children, indicating greater vulnerability due to lower body weight and higher intake rates. The probabilistic risk estimates further reinforce the severity of contamination, exceeding acceptable regulatory thresholds.

From a socio-economic perspective, the reliance of local populations on untreated groundwater for drinking water exacerbates exposure risks. The findings underscore the urgent need for regulatory enforcement, improved wastewater management, and the provision of alternative potable water sources. Without intervention, long-term exposure may result in an increased incidence of chronic health conditions, thereby imposing significant healthcare and economic burdens on affected communities.

Study Limitations

Like any other study, this work has limitations that are worth noting when interpreting the findings. With 15 samples, fine-scale spatial contamination patterns were not fully captured, and this sparsity might undermine the robustness of the multivariate statistical analyses. The interpolations were validated through cross-validation; however, a denser sampling grid in future studies would enhance geostatistical insights and better delineate pollution hotspots and their health implications.

Seasonal variations in groundwater chemistry were also not considered, which could influence contaminant transport and concentrations, possibly affecting the overall characterisation of exposure risks, particularly regarding the bioavailability and toxicity of contaminants over time. Furthermore, chromium speciation was not performed; total Cr was conservatively treated as entirely hexavalent (Cr^{6+}) for cancer risk calculations. This approach likely yields upper-bound estimates, as Cr^{6+} represents the toxicologically relevant fraction. Future studies incorporating year-round sampling and chromium speciation would provide more refined toxicity profiles and improved risk estimates.

Risk Management and Regulatory Implications

The probabilistic findings carry direct implications for groundwater regulation. Mitigation strategies should prioritise source control over point-of-use treatments alone, as arsenic accounts for approximately 48% of the total risk variance. Compulsory pre-treatment of brewery effluent and the installation of impermeable effluent storage systems would significantly reduce dissolved metal concentrations and prevent infiltration, thereby mitigating groundwater risk. Routine monitoring of shallow wells located within a 1 km downgradient radius of the brewery is strongly advisable. Moreover, public health advisories aimed at vulnerable populations, especially children, should be enforced until pollutant levels fall below regulatory limits.

Incorporating probabilistic risk assessment into Nigeria's groundwater management framework could improve decision-making, moving beyond the limitations of deterministic guideline exceedance assessments alone.

Conclusions

This study presents a comprehensive assessment of groundwater contamination in a brewery-impacted area of Aba, southeastern Nigeria, addressing both geochemical and public health dimensions. Across multiple sampling locations, groundwater exhibited elevated arsenic (As) and chromium (Cr) concentrations that exceed WHO guideline limits, whereas cadmium (Cd), cobalt (Co), nickel (Ni), and lead (Pb) generally remained within acceptable ranges. Multivariate statistical analyses, including PCA and correlation analysis, identified a two-source contamination signature. Cadmium (Cd) and cobalt (Co) are predominantly associated with geogenic sources within the Benin Formation, while As, Cr, Ni, and Pb are largely attributable to anthropogenic inputs from brewery effluents and associated industrial activities.

Probabilistic modelling revealed upper-bound exposure scenarios that substantially exceed deterministic averages, underscoring the importance of uncertainty quantification in groundwater risk assessment. Reliance solely on mean-based deterministic approaches could lead to an underestimate of threats to vulnerable populations.

Sensitivity analysis demonstrated that arsenic accounts for 48% of the total risk variance, directly linking public health outcomes to wastewater management practices. These findings call for mandatory pre-treatment of industrial effluents, routine monitoring in industrial areas, and full compliance with NESREA discharge guidelines.

The integration of hydrogeochemical characterisation, multivariate source apportionment, spatial risk mapping, and probabilistic modelling provides a robust, risk-based framework applicable to industrialising regions across sub-Saharan Africa. Future research should incorporate seasonal sampling, chromium speciation, and refined geostatistical approaches to improve predictive accuracy.

This study provides substantial evidence that inadequate industrial waste management poses significant risks to human health, highlighting the need for risk-based regulations and strengthened groundwater protection in rapidly urbanising areas.

References

Alloway, B. J. (Ed.). (2013). *Heavy metals in soils: Trace metals and metalloids in soils and their bioavailability* (3rd ed.). Springer Dordrecht. https://doi.org/10.1007/978-94-007-4470-7

Baird, R. B., Eaton, A. D., & Rice, E. W. (Eds.). (2017). *Standard methods for the examination of water and wastewater* (23rd ed.). American Public Health Association; American Water Works Association; Water Environment Federation. https://openlibrary.org/works/OL24518317W

Bamigboye, O. S., Omorinoye, O. A., Bamidele, T. E., & Umar, H. A. (2025). Granulometric and geochemical analyses of stream sediments from part of southwestern Nigeria: implication for mineralization potential. *International Journal of Earth Sciences Knowledge and Applications, 7*(2), 208–222. https://doi.org/10.5281/zenodo.17020942

Benkhelil, J. (1989). The origin and evolution of the Cretaceous Benue Trough (Nigeria). *Journal of African Earth Sciences (and the Middle East), 8*(2-4), 251–282. https://doi.org/10.1016/s0899-5362(89)80028-4

Foster, S. S. D., & Chilton, P. J. (2003). Groundwater: the processes and global significance of aquifer degradation. *Philosophical Transactions of the Royal Society of London. Series B: Biological Sciences, 358*(1440), 1957–1972. https://doi.org/10.1098/rstb.2003.1380

Gleick, P. H. (2014). Water, Drought, Climate Change, and Conflict in Syria. *Weather, Climate, and Society, 6*(3), 331–340. https://doi.org/10.1175/wcas-d-13-00059.1

IARC Working Group on the Evaluation of Carcinogenic Risks to Humans. (2012). *Arsenic, metals, fibres, and dusts* (IARC Monographs on the Evaluation of Carcinogenic Risks to Humans, Vol. 100C). International Agency for Research on Cancer. https://publications.iarc.who.int/120

Kabir, M. M., Hossain, N., Islam, A. R. M. T., Akter, S., Fatema, K. J., Hilary, L. N., Hasanuzzaman, M., Didar-ul-Alam, M., & Choudhury, T. R. (2021). Characterization of groundwater hydrogeochemistry, quality, and associated health hazards to the residents of southwestern Bangladesh. *Environmental Science and Pollution Research, 28*(48), 68745–68761. https://doi.org/10.1007/s11356-021-15152-2

Li, C., Zhou, X., Li, J., Liu, L., Su, H., Li, Y., He, M., Dong, J., Tian, J., Zhou, H., Gao, G., Zhang, C., & Luo, Z. (2022). Hydrogeochemical characteristics of thermal springs in the Qilian–Haiyuan fault zone at the northeast Tibetan Plateau: Role of fluids and seismic activity. *Frontiers in Earth Science, 10*. https://doi.org/10.3389/feart.2022.927314

Ochommadu, K. K., Ezere, U. A., Ikeme, C., Onwubuariri, C. N., & Onwurah, B. O. (2025). Heavy metal contamination in sediments and water near brewery effluent discharge sites: Implications for groundwater quality. *Applied Sciences, Computing, and Energy, 2*(2), 167–180. https://cemrj.com/index.php/volumes/article/view/18

Onwubuariri, C. N., Wasinda, I. G., Aigba, P. I., & Dinneya, O. C. (2025). Geophysical and geochemical evaluation and assessment of subsurface mineralisation in the Okokoma area, Cross River State, *Southeastern Nigeria. Journal of Earth Science Biointerfaces, 1*(1), 1–11. https://www.usodpublishers.com/JESB/USOD-JESB-1002.pdf

Orosun, M. M., Adewuyi, A. D., Salawu, N. B., Isinkaye, M. O., Orosun, O. R., & Oniku, A. S. (2020). Monte Carlo approach to risk assessment of heavy metals at automobile spare part and recycling market in Ilorin, Nigeria. Scientific Reports, 10, 22084. https://doi.org/10.1038/s41598-020-79141-0

Orosun, M. M., Enemuwe, C. A., Usikalu, M. R., Salawu, N. B., Abdulraheem, I. A., Udouso, V. B., Adagunodo, T. A., Babarimisa, I. O., Akinpelu, A., & Achuka, J. A. (2021). Natural radionuclide and radiological impact assessment of teak plantation, University of Ilorin, Kwara State. In *IOP Conference Series: Earth and Environmental Science* (Vol. 665, No. 1, p. 012044). IOP Publishing. https://doi.org/10.1088/1755-1315/665/1/012044

Rinklebe, J., Antoniadis, V., Shaheen, S. M., Rosche, O., & Altermann, M. (2019). Health risk assessment of potentially toxic elements in soils along the Central Elbe River, Germany. *Environment International, 126*, 76–88. https://doi.org/10.1016/j.envint.2019.02.011

Sims, K. W. W., Goldstein, S. J., Blichert-toft, J., Perfit, M. R., Kelemen, P., Fornari, D. J., Michael, P., Murrell, M. T., Hart, S. R., DePaolo, D. J., Layne, G., Ball, L., Jull, M., & Bender, J. (2002). Chemical and isotopic constraints on the generation and transport of magma beneath the East Pacific Rise. *Geochimica et Cosmochimica Acta, 66*(19), 3481–3504. https://doi.org/10.1016/s0016-7037(02)00909-2

Smedley, P. L., & Kinniburgh, D. G. (2017). Molybdenum in natural waters: A review of occurrence, distributions and controls. *Applied Geochemistry, 84*, 387–432. https://doi.org/10.1016/j.apgeochem.2017.05.008

Smith, D. B., & Reimann, C. (2008). Low-density geochemical mapping and the robustness of geochemical patterns. *Geochemistry: Exploration, Environment, Analysis, 8*(3-4), 219–227. https://doi.org/10.1144/1467-7873/08-171

Twinomucunguzi, F. R. B., Nyenje, P. M., Kulabako, R. N., Semiyaga, S., Foppen, J. W., & Kansiime, F. (2020). Reducing Groundwater Contamination from On-Site Sanitation in Peri-Urban Sub-Saharan Africa: Reviewing Transition Management Attributes towards Implementation of Water Safety Plans. *Sustainability, 12*(10), 4210. https://doi.org/10.3390/su12104210

U.S. Environmental Protection Agency. (2001). *Methods for collection, storage, and manipulation of sediments for chemical and toxicological analyses: Technical manual (EPA-823-B-01-002)*. Office of Water, U.S. Environmental Protection Agency. Washington, DC. https://purl.org/scimeta/EPA-823-B-01-002

U.S. Environmental Protection Agency. (2007). *Framework for metals risk assessment (EPA-120-R-07-001)*. Risk Assessment Forum, Office of the Science Advisor. U.S. Environmental Protection Agency. https://purl.org/scimeta/EPA-120-R-07-001

U.S. Environmental Protection Agency. (2011). *Exposure Factors Handbook: 2011 edition (EPA/600/R-09/052F)*. National Center for Environmental Assessment, Office of Research and Development, U.S. EPA, Washington, DC. https://purl.org/scimeta/EPA-600-R-09-052F

Ubong, U. U., Ekwere, I. O., Ikpe, E. E., & Obadimu, C. (2023). (2023). Evaluation of Heavy Metals and Total Hydrocarbon Contents in Crassostrea Spp (Oysters) from Qua Iboe River, Ibeno LGA. *American Journal of Applied and Industrial Chemistry, 7*(1), 17-24. https://doi.org/10.11648/j.ajaic.20230701.13

World Health Organization. (2017). *Guidelines for drinking-water quality* (4th ed.). WHO Press. https://www.who.int/publications/i/item/9789241549950